Bangladesh Pharmaceutical Journal ***29****(2): 172-192, 2026 (July)*

Structure-Based *In Silico* Screening of PubChem Compounds for Potential Anti-Inflammatory and Anticancer Targets

Mst Neha Islam Ema[1], A.B.M. Ashraful[2], Kanij Fatema[1], Saikat Bhowmik[1], A.H.M. Khurshid Alam[3] and Farhad Hossain[1]

[1]Department of Pharmacy, State University of Bangladesh, Dhaka-1461, Bangladesh
[2]Department of Pharmacy, R. P. Shaha University, Narayanganj-1400, Bangladesh
[3]Department of Pharmacy, University of Rajshahi, Rajshahi-6205, Bangladesh

(Received: November 14, 2025; Accepted: January 26, 2026; Published (web): July 20, 2026)

Abstract

Multi-target treatment methods are essential because inflammation and cancer involve intricate, interrelated pathways. To screen thirty different small compounds from PubChem for potential multi-target activity, this study employed a structure-based drug design approach. Their binding affinities for key inflammatory, analgesic and carcinogenic protein targets were evaluated using molecular docking, yielding promising candidates for further experimental validation. A total of eight pharmacologically significant receptors were selected: COX-1 (3KK6), COX-2 (3LN1), MOR (4DKL), EGFR (4HJO), ERα (3ERT), AR (1E3G), HER2 (3PP0), and CDK8 (5F19) targets. Protein structures were prepared using Discovery Studio and molecular docking was performed with AutoDock Vina in PyRx. Standard drugs such as aspirin, tramadol, erlotinib, tamoxifen, bicalutamide, lapatinib and raltitrexed were used for comparative evaluation of docking scores and interaction patterns. Post-docking analysis primarily focused on key amino acid interactions, hydrophobic contacts and hydrogen bonding. Among all tested compounds, C25, was identified as the most potent and effective compound. It exhibited strong binding affinities toward 3LN1 (-10.0 kcal/mol), 3PP0 (-9.6 kcal/mol), 5F19 (-11.9 kcal/mol), 3ERT (-8.6 kcal/mol), 1E3G (-8.8 kcal/mol), 4HJO (-8.9 kcal/mol), surpassing their respective standards. Moreover, Verimol K with 3KK6 (-7.8 kcal/mol) and 8-Deoxylactucin with 4DKL (-7.5kcal/mol) showed notable activity. Overall, the pyrazolin derivative represents a novel multi-target ligand with potential applications as an anti-inflammatory, analgesic and anti-neoplastic agent. Its strong binding affinity across multiple therapeutic targets highlights its promise as a lead scaffold for future drug development.

Key words: Lung cancer, breast cancer, stomach cancer, inflammation, PubChem, ADMET.

Introduction

Chronic inflammation is a fundamental key to diseases, including cancer, autoimmune disorders, and metabolic diseases that promote genomic instability, angiogenesis, and cellular transformation, ultimately tumor progression (Greten and Grivennikov, 2019). Inflammatory mediators such as TNF-α, IL-6, NF-κB, and COX-2 play central roles in chronic inflammation to tumorigenesis, thereby positioning anti-inflammatory targets as promising cancer therapy (Wen *et al.*, 2022). Despite major advancements in immunotherapy, safe discovery remains costly and has low success rates. Traditional high-throughput screening (HTS) approaches are expensive and often yield high false-positive rates. Structure-based *in silico* drug discovery enhances screening efficiency by minimizing the number of compounds that need experimental validation (Zhao, 2024).

Structure-based virtual screening combines docking, interaction analysis, and rescoring to predict binding affinity and prioritize active compounds, with recent advances in algorithms, protein flexibility, and hybrid scoring improving its

Corresponding authors: Farhad Hossain, E-mail: fhayon07@gmail.com; Phone Number: +8801701009374
Dr. A. H. M. Khurshid Alam; E-mail: khurshid.jaist@gmail.com; Phone Number: +8801719634499
DOI: https://doi.org/10.3329/bpj.v29i2.91855

reliability (Agu *et al.,* 2023). These computational approaches have successfully identified leads for cancer and inflammation-related targets such as kinases, inflammatory enzymes, cytokine receptors, and epigenetic regulators, while PubChem provides a vast, diverse chemical libraries that enable efficient structure-based screening (Kim *et al.*, 2019). PubChem's open access and standardized data formats allow seamless integration into *in silico* workflows, including molecular docking, ADMET analysis, and drug-likeness evaluation. Its incorporation into advanced SBVS approaches has accelerated early drug discovery, while multi-step strategies combining docking, MM-GBSA, molecular dynamics, and ADMET profiling enhance the reliability of hit identification (Uddin *et al*., 2022). By applying sequential computational filters, compounds with optimized physicochemical properties, stable binding, and favorable pharmacokinetics can be identified before experimental validation. Cancer progression, inflammation, and pain are mechanistically interconnected through overlapping molecular pathways involving inflammatory mediators, hormone receptors, and growth factor signaling. Chronic inflammation activates transcription factors such as NF-κB and STAT3, which regulate oncogenic targets including ERα, AR, EGFR, CDK8, and HER2, thereby promoting tumor initiation and progression (Lee *et al.,* 2022, Sokołowska *et al.,* 2024). Cyclooxygenase enzymes COX-1 and COX-2 further link inflammation to cancer by producing prostaglandin E_2 (PGE_2), which enhances proliferation, angiogenesis, and immune evasion, while also sensitizing nociceptive pathways (Millanta *et al.,* 2016). These inflammatory mediators also engage central analgesic pathways, including the μ-opioid receptor, whose expression and activity are altered under inflammatory conditions, thereby linking inflammation with pain (Wangzhou *et al.,* 2021).

Considering the mechanistic overlap between inflammation and carcinogenesis, structure-guided identification of small molecules capable of modulating these targets holds considerable therapeutic promise (Greten and Grivennikov, 2019, Wen *et al.,* 2022). This study applies a comprehensive structure-based *in silico* screening of chemically diverse compounds from PubChem against validated inflammatory and oncogenic targets. The integrated workflow, including multi-stage docking, binding energy analysis, pharmacokinetic prediction, and drug-likeness assessment, is used to identify potential anti-inflammatory and anticancer activity and prioritize candidates suitable for future *in vitro* and *in vivo* validation.

Materials and Methods

Pharmacokinetic (ADMET) and drug-likeliness analysis

The bioactive compounds retrieved from the PubChem database (https://pubchem.ncbi.nlm.nih.gov/) were subjected to comprehensive *in silico* analyses to assess their pharmacokinetic behavior, safety profiles, and overall drug-likeness before molecular docking studies. Evaluating ADMET (absorption, distribution, metabolism, excretion, and toxicity) properties is a critical step in drug discovery, as it allows the identification of compounds with favorable pharmacokinetics, minimal toxicity, and a higher likelihood of success as therapeutic agents. These predictions are necessary to determine whether a compound possesses the essential characteristics of a viable drug candidate, and only those meeting these criteria were selected for further investigation. ADMET profiling was performed using the pkCSM web server (http://biosig.unimelb.edu. au/pkcsm/ prediction), which applies graph-based molecular signatures to estimate key pharmacological and toxicological parameters. In parallel, the SwissADME tool (http://www.sib.swiss) was employed to evaluate drug-likeness, including lipophilicity, solubility, permeability, bioavailability, and compliance with established medicinal chemistry rules. This step ensures that compounds with optimal physicochemical and pharmacokinetic properties are prioritized for subsequent analyses. Following these evaluations, the selected compounds were converted into canonical SMILES format using the PubChem database, enabling their seamless integration into

molecular docking workflows to predict ligand–protein interactions and potential pharmacological activity.

Molecular Docking Study

Ligand Preparation: A total of 200 structurally diverse small-molecule compounds were initially explored and retrieved from the PubChem database (https://pubchem.ncbi.nlm.nih.gov/), a widely used open-access chemical repository for computational drug discovery (Kim *et al*., 2016). These compounds were selected broadly without restriction to any plant source to ensure wide chemical scaffold diversity and maximize the likelihood of identifying biologically active candidates.

For comparative validation of docking performance, well-established standard drugs were incorporated for each target receptor based on their recognized therapeutic relevance in cancer, inflammation, and analgesia. Tamoxifen was selected as the standard ligand for the estrogen receptor associated with breast cancer (Jordan, 2021). While Bicalutamide served as the androgen receptor standard for prostate cancer (Ghaffar *et al*., 2025). For stomach cancer, 5-Fluorouracil (5-FU) was employed due to its central role in gastric cancer chemotherapy (Ghaffar *et al*., 2025). Cetuximab was used as the reference molecule for colorectal cancer because of its inhibitory action on EGFR signaling (Allegra *et al*., 2016) and Erlotinib was selected as the standard for lung cancer computational studies owing to its established EGFR-targeted mechanism (Remon and Hendriks, 2021). Aspirin was employed as a classical standard for COX-1 and COX-2, respectively, in agreement with their well-documented selectivity profiles (Ahmadi *et al*., 2022). For the μ-opioid receptor (central analgesic target), Tramadol was used as the standard reference ligand based on its established μ-receptor agonistic activity (Miotto *et al*., 2017). These standard drugs allowed for comparative benchmarking of docking scores, thereby enabling accurate assessment of the binding efficiency and pharmacological potential of the selected candidate compounds (Azad, 2023). All compounds were subjected to drug-likeness and ADMET filtering**,** including Lipinski's Rule of Five, Veber parameters, Ghose filters, and key pharmacokinetic properties. From this screening, 50 compounds that satisfied major drug-likeness criteria and exhibited favorable ADMET profiles were shortlisted for detailed computational evaluation (Edache *et al.,* 2023, Prado-Romero *et al.,* 2023). The selected ligands were visualized and pre-processed using Discovery Studio (version 2020) to verify proper atom connectivity, valence corrections, and hydrogen assignments. Geometric optimization was performed to achieve stable, low-energy conformations. Energy minimization was performed using OpenBabel with the steepest descent algorithm to eliminate steric clashes and internal strain (Morris *et al.,* 2009, Yuan *et al.,* 2023). Finally, the optimized ligand structures were converted into PDBQT format for compatibility with AutoDock Vina in PyRx, ensuring accurate modeling of ligand flexibility, orientation, and conformational sampling during docking simulations (Goodsell *et al*., 2021).

Protein Preparation: The receptor proteins selected for molecular docking were chosen based on their well-established biological roles in inflammation modulation and cancer regulation. Three-dimensional (3D) crystal structures of the selected proteins were retrieved from the RCSB Protein Data Bank (Berman *et al*., 2000). All selected protein structures, determined by X-ray crystallography, were chosen due to their established roles in cancer, inflammation, and pain-related pathways. These targets include Human Epidermal Growth Factor Receptor 2 (HER2; PDB ID: 3PP0, 2.25 Å), associated with gastric cancer, Cyclin-Dependent Kinase 8 (CDK8; PDB ID: 5F19, 2.04 Å), linked to colorectal cancer, Estrogen Receptor Alpha (ERα; PDB ID: 3ERT, 1.90 Å) involved in breast cancer, Androgen Receptor (AR; PDB ID: 1E3G, 2.40 Å) related to prostate cancer, Epidermal Growth Factor Receptor (EGFR; PDB ID: 4HJO, 2.75 Å) implicated in lung cancer; the μ-opioid receptor (MOR; PDB ID: 4DKL, 2.80 Å), which plays a role in pain regulation and the inflammatory enzymes Cyclooxygenase-1 (COX-1; PDB ID: 3KK6, 2.75 Å)

and Cyclooxygenase-2 (COX-2; PDB ID: 3LN1, 2.40 Å). All crystal structures were opened and pre-processed in BIOVIA Discovery Studio (Discovery Studio Visualizer, 2020), where crystallographic water molecules, buffer ions, and non-protein heteroatoms were removed unless they represented functionally essential cofactors. Alternate location atoms were resolved to their primary occupancy states, while co-crystallized ligands were removed to prepare the proteins for docking, but retained temporarily to guide binding-site identification. Protonation states of titratable residues at physiological pH (7.0-7.4) were assigned using PROPKA3 (Olsson *et al*., 2011). Polar hydrogens were added to define hydrogen-bond geometries correctly. Local steric clashes were relieved through energy minimization in Swiss-PdbViewer 4.1.0 (Guex *et al*., 2009) using the GROMOS96 force field, applying short steepest-descent and conjugate-gradient steps until the RMS gradient reached below 0.02 kcal·mol^{-1}·Å^{-1}; backbone atoms were restrained to preserve the crystallographic fold while allowing side-chain relaxation around the binding site. Binding pockets were defined according to the location of co-crystallized ligands and supported by literature describing canonical active sites for each receptor (Kitchen *et al*., 2004). For AutoDock Vina/AutoDock docking, all receptors were converted to PDBQT format using AutoDock Tools (Morris *et al*., 2009). Where atom types, partial charges and rotatable bonds were appropriately assigned. For docking, stomach cancer receptor 3PP0 was prepared using a grid box with dimensions x = 19.29, y = 23.90, z = 10.56, centered at x = 15.31, y = 21.15, z = 26.85. The colorectal cancer receptor 5F19 used a grid box of x = 40.27, y = 33.87, z = 21.57, centered at x = 16.66, y = 48.91, z = 18.22. The breast cancer receptor 3ERT used a grid box of x = 15.27, y = 8.14, z = 28.04, centered at x = 27.38, y = -3.02, z = 23.37. The prostate cancer receptor 1E3G used a grid box of x = 35.52, y = 28.70, z = 19.01, centered at x = 1.48, y = 29.54, z = 8.12. The COX-1 receptor 3KK6 used a grid box of x = 14.44, y = 8.28, z = 22.44, centered at x = -30.68, y = 43.47, z = -2.69. The COX-2 receptor 3LN1 used a grid box of x = 26.74, y = 32.84, z = 19.57, centered at x = 72.42, y = -18.03, z = -4.54. The lung cancer receptor 4HJO used a grid box of x = 29.56, y = 39.47, z = 15.95, centered at x = 21.49, y = 26.51, z = 2.65. The μ-opioid receptor 4DKL used a grid box of x = 45.85, y = 24.26, z = 20.23, centered at x = -36.84, y = 66.21, z = 39.59. Throughout the receptor preparation workflow, rigorous structural quality checks such as validating hydrogen-bonding networks, inspecting side-chain orientations and confirming the integrity of residues lining the active site were performed to ensure consistency with experimentally determined binding modes (Kitchen *et al*., 2004). The final, validated PDBQT files were used for all docking simulations.

Molecular Docking and Interaction Analysis: Molecular docking simulations were performed using PyRx (version 0.8), an integrated virtual screening tool widely applied for structure-based drug discovery (Dallakyan and Olson, 2014). PyRx incorporates AutoDock Vina as its docking engine, which employs an empirical scoring function and an iterated local search global optimizer based on a hybrid Lamarckian evolutionary algorithm to estimate binding affinity (ΔG, kcal/mol) and predict optimal ligand orientations within the receptor's active site (Trott and Olson, 2010). Grid box centers and dimensions were defined individually for each target protein to ensure complete coverage of the binding pocket, thereby allowing flexible ligand positioning and exhaustive sampling of conformational space. All ligands were docked against each receptor to evaluate multi-target interaction potential, an approach increasingly emphasized in modern polypharmacology research (Anighoro *et al*., 2014). The docking parameters were optimized by adjusting the exhaustiveness value to ensure convergence, reproducibility, and high-accuracy predictions in accordance with recommended best practices for Vina-based screening workflows (Trott and Olson, 2010).

Following docking, the binding affinity scores were recorded for all ligand–protein complexes, and the top-ranked poses (lowest ΔG) were selected for post-docking analyses. The ligand-receptor

complexes were visualized using BIOVIA Discovery Studio Visualizer (2020), enabling detailed exploration of non-covalent interactions such as hydrogen bonds, hydrophobic contacts, van der Waals forces, electrostatic interactions, and π-π stacking, which are central to ligand stabilization within active pockets (Baroroh *et al.,* 2023, Kourat *et al.,* 2025). Functional groups responsible for molecular recognition and receptor-specific complementarity were systematically identified. Furthermore, interaction patterns of the highest-scoring PubChem compounds were compared against known reference drugs, including aspirin for anti-inflammatory activity and loperamide for gastrointestinal regulation, to ensure pharmacological relevance and docking reliability, a commonly recommended validation strategy in *in silico* pharmacology (Bagchi *et al*., 2025; Huggins *et al*., 2012).

Results and Discussion

A total of 200 compounds were initially obtained from the PubChem database to maintain structural diversity. These compounds underwent ADMET and drug-likeness evaluation using pkCSM and SwissADME, from which 50 compounds met the essential pharmacokinetic and medicinal chemistry properties. These shortlisted compounds were subsequently subjected to molecular docking. Among the docked compounds, the top 30 were shortlisted based on binding affinity and stability of key interactions, including hydrogen bonding. This systematic screening strategy facilitated the selection of compounds with promising drug-like attributes and potential biological significance.

The pkCSM-based ADMET profiling indicated overall favorable pharmacokinetics, including moderate solubility, reasonable Caco-2 permeability, high intestinal absorption, moderate VDss, low BBB/CNS penetration, minimal CYP-mediated metabolism, and acceptable clearance profiles, while toxicity predictions revealed moderate to relatively high acute toxicity (LD_{50}) alongside predominantly moderate *Tetrahymena pyriformis* and low minnow toxicity. The predicted toxicity may be attributed to increased lipophilicity and bulky fluorinated substituents, which can enhance membrane permeability and bioaccumulation. This issue can be addressed through structural optimization, such as reducing lipophilicity, introducing polar functional groups, and minimizing steric bulk to improve the safety profile while maintaining binding affinity. These findings are consistent with earlier reports demonstrating that computational ADMET models reliably identify compounds with acceptable absorption, distribution, metabolism and toxicity characteristics (Daina *et al*., 2017; Pires *et al*., 2015). 50 compounds were selected from the PubChem Database, and drug likeness properties were evaluated using SwissADME (Table 1). These assessments included parameters such as hydrogen bond acceptors (HBA), hydrogen bond donors (HBD), topological polar surface area (TPSA), aqueous solubility (Log S ESOL), and violations of Lipinski, Ghose, and Veber rules, in addition to bioavailability scores and synthetic accessibility (Table 2). The majority of the compounds (40 out of 50) conformed to Lipinski's Rule of Five, with only minimal violations observed in 10 compounds. Three compounds (C21, C36 and C39) exhibited Ghose violations, while eight compounds demonstrated Veber violations attributable to increased TPSA or a higher number of rotatable bonds. Bioavailability ranged from 0.17 to 0.85; the majority of compounds exhibited a value of 0.55, indicating favorable potential for oral absorption, while synthetic accessibility, spanning from 1.36 to 6.3, demonstrated moderate ease of synthesis. Compounds C1, C3, C4, C10, C11, and C15, as well as C35 and C41, exhibited no violations of any drug-likeness criteria and are promising candidates for oral bioavailability. A total of 50 matches were identified through this screening, which can be further utilized for *in silico* molecular docking targeting cancer and anti-inflammatory markers.

The ADMET profiling of 50 compounds chosen from those designed via pkCSM exhibited favorable pharmacokinetic properties and an absence of toxicity. The water solubility ranged from -7.59 to -

0.195 log mol/L, indicating moderate to low levels, while the Caco-2 permeability (log Papp) values fell between -0.42 and 1.83, suggesting at least reasonable potential for intestinal absorption in most compounds. The estimated human intestinal absorption ranged from 6.41% (C40) to 99.95% (C38), suggesting a high likelihood of oral bioavailability for the majority of compounds. The volume of distribution at steady state (VDss) indicated a moderate distribution, ranging from -1.57 to 0.578 (log L/kg). Most of the compounds exhibited low BBB and CNS permeability, indicating limited penetration into the central nervous system. In the metabolism inhibition study, none of these compounds demonstrated CYP2D6 inhibitory activity and only a limited subset (e.g., C3 and C10) inhibited CYP3A4, suggesting minimal metabolic liability.

Table 1. PubChem compounds canonical SMILES.

Compound serial	IUPAC name	Molecular weight (g/mol)	canonical smiles
C1	Verimol K	244.24	C1=CC=C(C=C1)COC(=O)C2=C(C=CC=C2O)O
C2	8-Deoxylactucin	260.28	C1=C2[C@@H]([C@@H]3[C@@H](CC1)C(=C)C(=O)O3)C(=CC2=O)CO
C3	(E)-3,3'-Dimethoxy-4,4'-dihydroxystilbene	272.3	COC1=C(C=CC(=C1)/C=C/C2=CC(=C(C=C2)O)OC)O
C4	1-(2,4-Dihydroxyphenyl)-2-(4-methoxy-3-nitrophenyl)ethanone	272.8	COC1=C(C=C(C=C1)CC(=O)C2=C(C=C(C=C2)O)O)[N+](=O)[O-]
C5	N-Benzyloxy-2,2-bis(trifluoromethyl)aziridine	285.19	C1C(N1OC(=O)C2=CC=CC=C2)(C(F)(F)F)C(F)(F)F
C6	L-Alanine, N-benzoyl-, methyl ester	207.22	C[C@@H](C(=O)OC)N(C1=CC(=C(C=C1)F)Cl)C(=O)C2=CC=CC=C2
C7	Phthalic acid, di(6-methylhept-2-yl) ester	390.56	C(C)CCCC(C)OC(=O)C1=CC=CC=C1C(=O)OC(C)CCCC(C)C
C8	3-Methylbenzoic acid, 2-formyl-4,6-dichlorophenyl ester	309.14	CC1=CC(=CC=C1)C(=O)OC2=C(C=C(C=C2Cl)Cl)C=O
C9	5-(2,2,2-Tri(2-cyanoethyl)acetyl)-2-methylpyridine	255.3	CC1=NC=C(C=C1)C(=O)C(CCC#N)(CCC#N)CCC#N
C10	Diethylmalonic acid, diphenethyl ester	312.36	CCC(CC)(C(=O)OCCC1=CC=CC=C1)C(=O)OCCC2=CC=CC=C2
C11	4,4'-Difluorobenzil	246.21	C1=CC(=CC=C1C(=O)C(=O)C2=CC=C(C=C2)F)F
C12	3-Hydroxy-4-methoxycinnamic acid	194.18	COC1=C(C=C(C=C1)/C=C/C(=O)O)O
C13	L-Phenylalanine, N-acetyl-, methyl ester	221.25	CC(=O)N[C@@H](CC1=CC=CC=C1)C(=O)OC
C14	9-Octadecenoic acid	282.46	CCCCCCCCC=CCCCCCCCC(=O)O
C15	Curcumenol	234.33	C[C@H]1CC[C@@H]2[C@]13CC(=C(C)C)[C@](O3)(C=C2C)O
C16	9,12,15-Octadecatrienoic acid, 2,3-dihydroxypropyl ester, (Z,Z,Z)-	352.51	CC/C=C\C/C=C\C/C=C\CCCCCCCC(=O)OCC(CO)O
C17	2,4-Bis(dimethylbenzyl)-6-t-butylphenol	389.6	CC(C)(C)C1=C(C(=CC(=C1)C(C)(C)C2=CC=CC=C2)C(C)(C)C3=CC=CC=C3)O
C18	2-Naphthyl methyl ketone	170.21	CC(=O)C1=CC2=CC=CC=C2C=C1
C19	Benzoic acid, 3,4,5-trihydroxy-, methyl ester	184.15	COC(=O)C1=CC(=C(C(=C1)O)O)O
C20	Isospathulenol	220.35	CC1=C2CCC(C2C3C(C3(C)C)CC1)(C)O
C21	Pentafluoropropionic anhydride	214.04	C(=O)(C(C(F)(F)F)(F)F)OC(=O)C(C(F)(F)F)(F)F
C22	Citronellyl butyrate	226.36	CCCC(=O)OCCC(C)CCC=C(C)C
C23	E-6-Octadecen-1-ol acetate	310.52	CCCCCCCCCCCC/C=C/CCCCCOC(=O)C
C24	Innuchenenolide C	266.34	CC1CC2C(C(C3(C1C(CC3OC(=O)C)OC(=O)C)C)O)C(=C)C(=O)O2

C25	2-Pyrazolin-5-ol, 1-acetyl-5-perfluoroctyl-3-methyl-		CC(NC1=NNC(C)=C(C(F)(F)F)C1=O)C(=O)N(C2=NNC(C)=C(C(F)(F)F)C2=O)C(=O)NC(C)=O
C26	9-Octadecene, 1,1-dimethoxy-, (Z)-	308.53	CCCCCCCC/C=C\CCCCCCCC(OC)OC
C27	(9E,11E)-Octadecadienoic acid	280.45	CCCCCC/C=C/C=C/CCCCCCCC(=O)O
C28	9-Octadecenoic acid, methyl ester, (E)-	296.49	CCCCCCCC/C=C/CCCCCCCC(=O)OC
C29	n-Hexadecanoic acid	256.43	CCCCCCCCCCCCCCCC(=O)O
C30	Methyl stearate	298.5	CCCCCCCCCCCCCCCCCC(=O)OC
C31	9,12-Octadecadienoic acid (Z,Z)-, methyl ester	294.48	CCCCC/C=C\C/C=C\CCCCCCCC(=O)OC
C32	Hexadecanoic acid, methyl ester	270.45	CCCCCCCCCCCCCCCC(=O)OC
C33	Z-(13,14-Epoxy)tetradec-11-en-1-ol acetate	268.39	CC(=O)OCCCCCCCCCC/C=C\C1CO1
C34	9,12,15-Octadecatrienoic acid, methyl ester, (Z,Z,Z)-	292.47	CC/C=C\C/C=C\C/C=C\CCCCCCCC(=O)OC
C35	p-Coumaric acid	164.16	C1=CC(=CC=C1/C=C/C(=O)O)O
C36	Gamma-sitosterol	414.71	CC[C@@H](CC[C@@H](C)[C@H]1CC[C@@H]2[C@@]1(CC[C@H]3[C@H]2CC=C4[C@@]3(CC[C@@H](C4)O)C)C)C(C)C
C37	Lactose	342.3	C([C@@H]1[C@@H]([C@@H]([C@H]([C@@H](O1)O[C@@H]2[C@H](OC([C@@H]([C@H]2O)O)O)CO)O)O)O)O
C38	Sarcosine, n-propargyloxycarbonyl-, propargyl ester	211.22	CN(CC(=O)OCC#C)C(=O)OCC#C
C39	D-Alanine, N-propargyloxycarbonyl-, propargyl ester	213.24	CC(C(=O)OCC#C)NC(=O)OCC#C
C40	1,2,4-Oxadiazole-3-(1-amino-2-aza-3-oxa-pent-2-en-4-one)	154.13	CC(=O)O/N=C(/C1=NOC=N1)\N
C41	trans-Sinapaldehyde	208.21	COC1=CC(=CC(=C1O)OC)/C=C/C=O
C42	N-Acetyl-phenylalanine methylester	207.23	CC(=O)N[C@H](CC1=CC=CC=C1)C(=O)OC
C43	Benzeneacetic acid, 4-hydroxy-3,5-dimethoxy-, methyl ester	226.23	COC1=CC(=CC(=C1O)OC)CC(=O)OC
C44	Propiophenone, 2,2',4',6'-tetramethyl-	194.29	CC1=CC(=C(C(=C1)C)C(=O)C(C)C)C
C45	Salicylic acid	138.12	C1=CC=C(C(=C1)C(=O)O)O
C46	5-Formyl-2-methoxyphenyl acetate	182.17	CC(=O)OC1=C(C=CC(=C1)C=O)OC
C47	L-Histidine, 3-methyl-	169.18	CN1C=NC=C1C[C@@H](C(=O)O)N
C48	Shikimic acid	174.15	C1[C@H]([C@@H]([C@@H](C=C1C(=O)O)O)O)O
C49	Coniferyl aldehyde	178.19	COC1=C(C=CC(=C1)/C=C/C=O)O
C50	Salicyl hydrazide	136.15	C1=CC=C(C(=C1)C(=O)NN)O

Cumulative urinary excretion aligned with complete nonrenal elimination, with total clearance ranging from -0.115 to 2.188 log ml/min/kg, and none being OCT2 substrates in the kidney (Table 3). Predictions of properties indicated that nearly all derivatives were non-mutagenic (AMES test negative), non-hERG I blockers, and non-hepatotoxic. Acute oral toxicity (LD_{50} = 1.42-4.33 mol/kg body weight) indicates that several compounds fall within a moderate to relatively high toxicity range. Accordingly, these compounds are better described as pharmacokinetically promising leads that need further optimization and experimental validation for toxicity reduction. Conversely, environmental toxicity predictions based on *Tetrahymena pyriformis* and minnow models showed generally low ecological risk for most compounds, suggesting a comparatively favorable environmental

Table 2. The result of drug-likeness with swiss ADME.

Compound serial	#H-bond acceptors	#H-bond donors	TPSA	ESOL Log S	Lipinski #violations	Ghose #violations	Veber #violations	Bioavailability score	Synthetic accessibility
C1	4	2	66.76	-3.54	0	0	0	0.55	1.78
C2	4	1	63.6	-1.52	0	0	0	0.55	4.19
C3	4	2	58.92	-4.18	0	0	0	0.55	2.24
C4	6	2	112.58	-3.58	0	0	0	0.55	2.52
C5	4	0	46.61	-3.8	0	0	0	0.55	2.54
C6	4	0	52.6	-5.84	1	1	1	0.55	4.01
C7	3	0	43.37	-4.72	0	0	0	0.55	2.36
C8	5	0	101.33	-1.89	0	0	0	0.55	2.26
C9	4	0	52.6	-5.25	1	0	1	0.55	2.81
C10	4	0	34.14	-3.92	0	0	0	0.55	1.57
C11	4	2	66.76	-2.11	0	0	0	0.85	1.9
C12	3	1	55.4	-1.67	0	0	0	0.55	2.03
C13	2	1	37.3	-5.41	1	1	1	0.85	3.07
C14	2	1	29.46	-2.7	0	0	0	0.55	5.73
C15	4	2	66.76	-2.7	0	0	0	0.55	5.73
C16	1	1	20.23	-7.6	1	1	0	0.55	2.97
C17	1	0	17.07	-3.06	0	0	0	0.55	1.87
C18	4	2	58.92	-4.18	0	0	0	0.55	2.24
C19	5	3	86.99	-1.73	0	0	0	0.55	1.5
C20	1	1	20.23	-2.86	0	0	0	0.55	4.35
C21	13	0	43.37	-3.55	0	3	0	0.55	2.94
C22	2	1	37.3	-5.7	1	1	1	0.55	3.28
C23	2	0	26.3	-3.55	0	0	0	0.55	4.88
C24	2	0	26.3	-5.7	1	1	1	0.17	4.13
C25	7	1	99.13	-3.03	0	0	0	0.55	3.67
C26	2	0	18.46	-5.7	1	1	1	0.85	2.31
C27	2	0	26.3	-5.32	1	1	1	0.55	2.76
C28	2	1	37.3	-5.02	1	0	1	0.55	2.76
C29	2	0	26.3	-5.83	1	1	1	0.55	2.53
C30	2	0	26.3	-5.83	1	1	1	0.55	3.6
C31	2	0	26.3	-5.18	1	1	1	0.55	3.6
C32	3	0	38.83	-3.49	0	0	1	0.85	1.61
C33	2	0	26.3	-3.49	0	0	1	0.55	6.3
C34	3	2	57.53	-2.02	0	0	0	0.17	5.41
C35	3	0	43.37	-2.51	0	0	0	0.55	2.8
C36	1	1	20.23	-7.9	1	3	0	0.55	3.17
C37	4	0	55.84	-0.85	0	0	0	0.55	2.14
C38	4	1	64.63	-0.99	0	0	0	0.55	2.03
C39	6	1	103.6	-0.82	0	3	0	0.55	1.93
C40	4	1	55.76	-2.04	0	0	0	0.55	1.36
C41	3	1	55.4	-1.67	0	0	0	0.85	1.48
C42	5	1	64.99	-2.01	0	0	0	0.55	1.76
C43	1	0	17.07	-3.56	0	0	0	0.55	2.47
C44	3	2	57.53	-2.5	0	3	0	0.55	1.88
C45	4	0	52.6	-1.73	0	0	0	0.55	1.98
C46	4	2	81.14	1.07	0	1	0	0.55	2.09
C47	3	1	46.53	-2.04	0	0	0	0.55	1.98
C48	3	3	75.35	-1.43	0	3	0	0.55	2.94
C49	2	1	52.6	-5.83	0	0	0	0.55	3.28
C50	1	2	81.14	-5.18	0	0	0	0.55	4.88

Table 3. The results of the ADME test with pkCSM.

Compound serial	Absorption			Distribution			Metabolism		Excretion	
	Water solubility (log mol/L)	Caco2 permeability (log Papp in 10^{-6} cm/s)	Intestinal absorption %	VDss (log L/kg)	BBB permeability	CNS permeability	CYP2D6 inhibitor	CYP3A4 inhibitor	Total clearance (log ml/min/kg)	Renal OCT2 substrate
C1	-2.93	1.05	92.66	-0.27	0.368	-2.322	No	No	0.448	No
C2	-2.06	0.48	86.91	0.009	-0.189	-2.952	No	No	0.533	No
C3	-3.54	1.28	90.51	0.125	0.151	-2.197	No	Yes	0.066	No
C4	-3.3	-0.42	78.24	-0.428	-0.239	-2.671	No	No	0.332	No
C5	-4.37	1.83	91.32	-0.204	0.118	-2.54	No	No	-0.115	No
C6	-4.92	1.45	95.6	-0.48	0.042	-1.539	No	No	0.076	No
C7	-6.5	1.41	91.59	0.253	-0.096	-2.061	No	No	1.659	No
C8	-4.34	0.98	88.43	0.022	-0.461	-2.858	No	No	1.818	No
C9	-5.79	1.06	94.91	0.124	0.598	-2.342	No	Yes	0.589	No
C10	-3.93	1.7	95.65	-0.425	0.416	-1.46	No	No	0.426	No
C11	-2.78	0.25	94.92	-1.195	-0.272	-2.535	No	No	0.617	No
C12	-1.7	1.18	83.86	0.132	-0.107	-2.683	No	No	0.782	No
C13	-5.92	1.56	91.82	-0.558	-0.168	-1.654	No	No	1.884	No
C14	-3.17	1.19	95.27	0.355	0.531	-2.609	No	No	1.016	No
C15	-5.79	0.45	91.75	-0.356	-0.83	-3.207	No	No	2.188	No
C16	-6.48	0.95	94.15	0.052	0.648	-1.183	No	No	0.646	No
C17	-3.55	1.21	96.2	0.372	0.414	-1.596	No	No	0.235	No
C18	-2.11	-0.11	74.4	-0.479	-0.606	-3.214	No	No	0.218	No
C19	-1.75	1.01	71.21	0.262	-1.03	-3.368	No	No	0.666	No
C20	-4	1.49	94.5	0.578	0.603	-2.546	No	No	0.881	No
C21	-3.53	1.432	88.954	-0.647	0.273	-3.316	No	No	0.581	No
C22	-5.924	1.563	91.823	-0.558	-0.168	-1.654	Yes	No	1.927	No
C23	-4.322	1.525	95.098	0.227	0.625	-2.192	No	No	1.618	No
C24	-7.594	1.606	91.735	0.332	0.786	-1.615	Yes	No	1.996	No
C25	-3.737	0.527	90.787	-0.087	-0.627	-3.003	No	No	1.118	No
C27	-2.641	-0.372	56.573	-0.911	-2.515	-4.557	No	No	0.362	No
C28	-5.862	1.57	92.329	-0.587	-0.142	-1.6	Yes	No	1.933	No
C29	-7.436	1.605	92.154	0.299	0.777	-1.516	Yes	No	1.981	No
C30	-5.562	1.558	92.004	-0.543	-0.111	-1.816	No	No	1.763	No
C31	-7.51	1.598	91.648	0.325	0.787	-1.569	Yes	No	1.929	No
C32	-7.343	1.612	92.66	0.272	0.767	-1.463	Yes	No	2.032	No
C33	-6.927	1.6	92.335	0.334	0.749	-1.678	Yes	No	1.861	No
C34	-4.711	1.661	95.058	0.198	-0.034	-2.242	No	No	1.652	Yes
C35	-7.232	1.619	93.166	0.246	0.757	-1.41	Yes	No	2.086	No
C36	-2.378	1.21	93.494	-1.151	-0.225	-2.418	No	No	0.662	No
C37	-3.137	1.287	99.945	0.178	0.085	-2.574	Yes	No	0.541	No
C38	-6.773	1.201	94.464	0.193	0.781	-1.705	No	No	0.628	No
C39	-0.72	-0.12	6.412	0.203	-1.024	-4.683	No	No	1.545	No
C40	-0.195	1.171	97.691	-0.346	-0.169	-2.952	No	No	0.84	No
C41	-0.382	0.639	89.193	-0.3	-0.233	-2.967	No	No	0.804	No
C42	-2.318	-0.169	76.11	-0.406	-0.558	-3.203	No	No	0.534	No
C43	-1.805	1.275	93.693	0.035	-0.195	-2.522	Yes	No	0.191	No
C44	-1.209	1.231	77.995	-0.193	-0.068	-2.623	No	No	0.79	No
C45	-1.752	0.472	89.436	-0.129	-0.291	-2.714	Yes	No	0.692	No
C46	-3.705	1.367	95.861	0.442	0.426	-1.74	Yes	No	0.342	No
C47	-1.808	1.151	83.887	-1.57	-0.334	-3.21	No	No	0.607	No
C48	-1.795	1.271	97.045	-0.397	-0.203	-2.511	Yes	No	0.745	No
C49	-2.891	0.612	82.061	-0.224	-0.564	-3.446	No	No	0.506	No
C50	-0.522	-0.23	46.681	-0.618	-0.683	-3.58	No	No	0.688	No

Table 4. The results of the toxicity test with pkCSM.

Compound serial	Toxicity						
	AMES toxicity	Max. tolerated dose (human) (log mg/kg/day)	hERG I inhibitor	Oral Rat Acute Toxicity (LD50) (mol/kg)	Hepatotoxicity	*T. Pyriformis* toxicity (log ug/L)	Minnow toxicity (log mM)
C1	No	0.04	No	2.06	No	1.15	0.62
C2	No	0.46	No	1.89	No	0.32	2.11
C3	No	0.33	No	2.07	No	1.21	0.83
C4	Yes	0.3	No	2.3	No	0.42	0.08
C5	No	0.74	No	2.65	No	0.63	0.18
C6	No	1.26	No	1.44	No	0.89	-2.57
C7	No	0.83	No	2.37	No	1.63	-0.02
C8	No	0.87	No	2.02	Yes	1.13	-0.28
C9	No	1.05	No	1.7	Yes	0.48	-3.1
C10	No	1.01	No	2.14	No	1.17	1.11
C11	No	1.45	No	2.3	No	0.27	2.1
C12	No	0.43	No	2.05	No	0.52	1.42
C13	No	-0.81	No	1.42	No	0.68	-1.44
C14	No	0.2	No	2.03	No	0.84	1.16
C15	No	0.04	No	1.71	No	0.7	-0.59
C16	No	0.58	No	3.42	No	0.29	-2.6
C17	No	0.68	No	2.09	No	0.77	0.45
C18	No	0.77	No	2.15	No	-0.29	2.81
C19	No	-0.31	No	1.92	No	0.15	2.72
C20	No	0.14	No	1.69	No	1.11	1.02
C21	No	0.395	No	4.329	No	1.038	2.262
C22	No	-0.81	No	1.417	No	0.676	-1.438
C23	No	0.646	No	1.818	No	1.997	-0.119
C24	No	-0.088	No	1.663	No	1.417	-1.892
C25	No	0.911	No	2.745	Yes	0.285	4.604
C26	No	-0.02	No	1.651	No	1.336	-1.986
C27	No	-0.827	No	1.429	Yes	0.701	-1.31
C28	No	0.04	No	1.637	No	1.529	-1.727
C29	No	-0.708	No	1.44	No	0.84	-1.083
C30	No	0.099	No	1.656	No	1.448	-1.854
C31	No	-0.019	No	1.617	No	1.603	-1.6
C32	No	0.178	No	1.635	No	1.935	-1.373
C33	No	0.164	No	1.607	No	2.09	-1.287
C34	No	-0.078	No	1.596	No	1.668	-1.473
C35	No	1.111	No	2.155	No	0.319	1.607
C36	No	0.297	No	1.927	No	0.733	1.161
C37	No	-0.621	No	2.552	No	0.43	-1.802
C38	No	1.442	No	1.643	No	0.285	9.052
C39	No	0.87	No	2.476	No	0.075	2.653
C40	No	0.834	No	2.297	No	0.235	2.945
C41	No	0.709	No	2.342	No	-0.091	2.591
C42	No	0.683	No	2.071	No	0.602	1.772
C43	No	0.904	No	2.259	No	0.701	2.071
C44	No	0.555	No	1.999	No	0.525	2.013
C45	No	0.834	No	1.798	No	1.357	0.1
C46	No	0.61	No	2.282	No	0.263	1.812
C47	No	1.276	No	2.414	No	0.48	1.628
C48	No	0.994	No	1.156	No	0.263	4.048
C49	No	1.12	No	1.958	No	0.655	1.798
C50	No	1.509	No	2.737	No	0.005	2.684

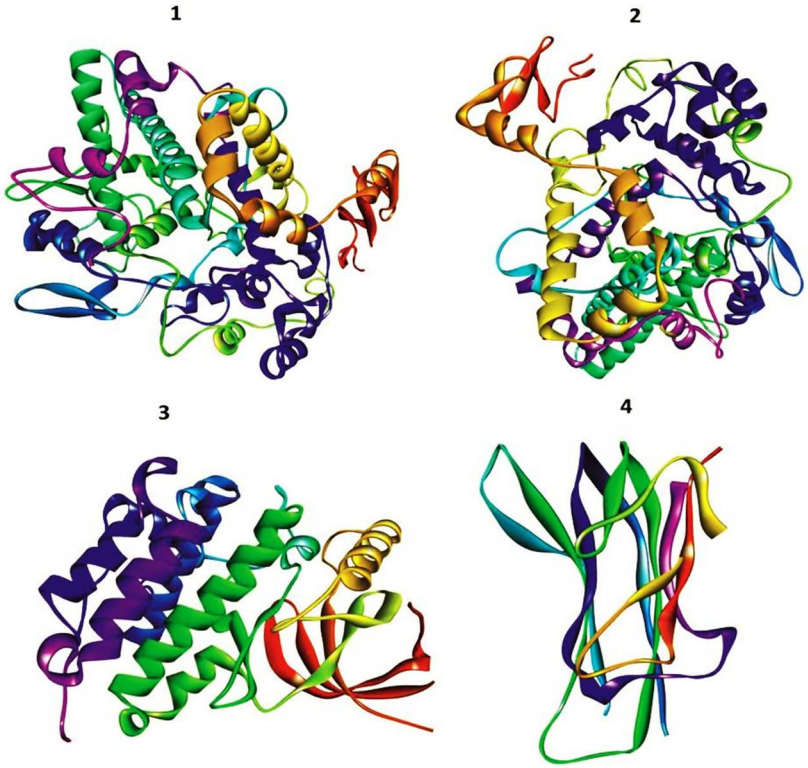

Figure 1. Three-dimensional structures of the four protein receptors: (1) COX-1 (3KK6), (2) COX-2 (3LN1), (3) lung cancer target EGFR (PDB: 4HJO) (4) μ-Opioid receptor (PDB: 4DKL).

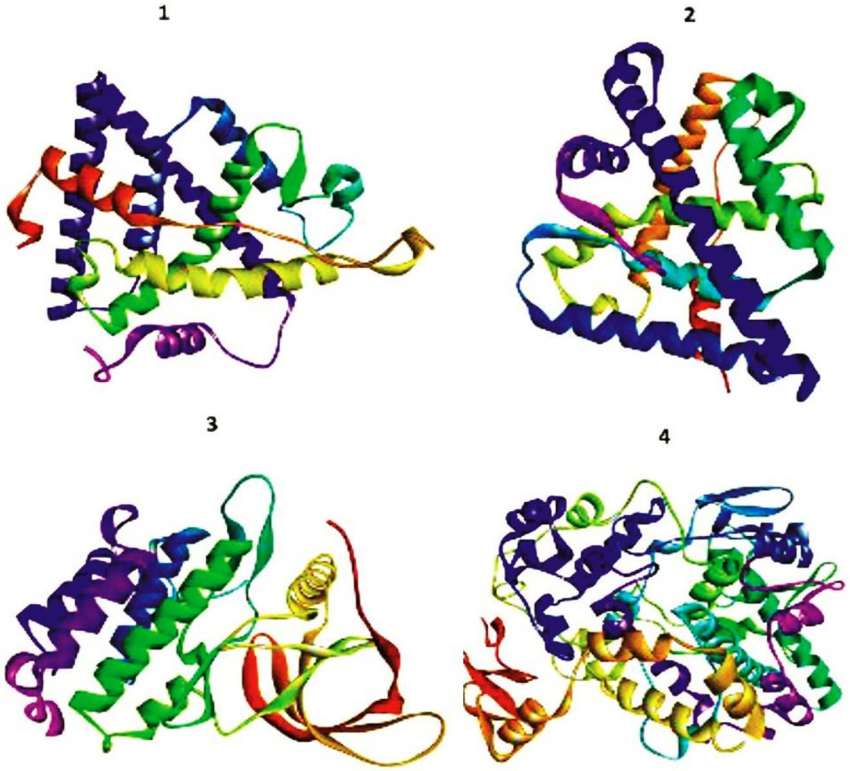

Figure 2. Three-dimensional structures of the four protein receptors: (1) Breast Cancer ERα (PDB: 3ERT), (2) Prostate Cancer AR (PDB: 1E3G), (3) Stomach Cancer target (PDB: 3PP0), (4) Colorectal Cancer CDK8 (PDB: 5F19).

safety profile, which is increasingly important in modern drug discovery. Furthermore, *T. pyriformis* and minnow toxicity predictions also indicated that the majority of the compounds are environmentally safe. The preceding analysis demonstrated that the 50 compounds possess favorable pharmacokinetic and pharmacodynamic properties, ensuring safety and are suitable for binding with PDK1 *in silico* molecular docking (Table 4).

Molecular docking studies of the 30 selected PubChem-derived compounds were performed against eight therapeutic protein targets depicted in **Figure (1, 2)**. COX-1 (3KK6), COX-2 (3LN1), EGFR (4HJO), MOR (4DKL), ERα (3ERT), AR (1E3G), HER2 (3PP0), and CDK8 (5F19), with several compounds exhibiting favorable predicted binding affinities and suggesting putative multi-target, anticancer and analgesic potential. The significant inhibitory effects on COX-1 and COX-2 are consistent with a potential anti-inflammatory activity, as the established roles of COX enzymes in prostaglandin synthesis are associated with inflammation (Ricciotti and FitzGerald, 2011, Ju *et al.,* 2022). With regard to the anti-inflammatory enzymes, the most effective Verimol K against COX-1 (3KK6) exhibited a binding affinity of -7.8 kcal/mol and engaged in interactions with Ile523, forming one hydrogen bond. This affinity surpasses that of aspirin, which demonstrated a binding affinity of -6.3 kcal/mol and also formed one hydrogen bond. Against COX-2 (3LN1), 1-acetyl-5-perfluoroctyl-3-methyl-6H-pyrazolin- exhibited affinities of -10.0 kcal/mol, forming two hydrogen bonds with Tyr341 and Met508. This performance significantly surpasses that of aspirin (-6.6 kcal/mol), as detailed in Table 5, in aqueous solution. The docking on the MOR (4DKL) yielded moderate affinity values ranging from -5.3 to -7.5 kcal/mol, with significant interactions involving Trp318, Asn127, and His54, resulting in interaction energies surpassing that of the standard drug tramadol (5.1 kcal/mol). While the MOR exhibited only moderate affinity relative to anti-inflammatory and anticancer targets binding affinities from -5.3 to -7.5 kcal/mol, which surpasses that of the reference analgesic tramadol (-5.1 kcal/mol), indicates potential neuro-modulatory effects. Nevertheless, opioid-related interactions must be thoroughly assessed due to the potential for off-target effects.

Furthermore, the compound's selective affinity for cancer-associated receptors-EGFR in lung cancer (4HJO), ERα in breast cancer (3ERT), AR in prostate cancer (1E3G) and CDK8 in colorectal cancer (5F19) indicates a potential role for this ligand as an oncological therapeutic. Inhibition of EGFR and CDK8 has been extensively documented as an effective strategy to suppress tumor proliferation, angiogenesis and transcriptional reprogramming (Yin *et al.,* 2024). The formation of multiple hydrogen bonds with the Human Epidermal Growth Factor Receptor 2 HER2 in stomach cancer target (3PP0) and CDK8 further corroborates robust stabilization within the ATP-binding sites, aligning with pharmacophores identified in previously characterized CDK inhibitors (Lin *et al.,* 2022). Such multi-target interactions are valuable because polypharmacology has been demonstrated to address drug resistance mechanisms and extend therapeutic efficacy in complex diseases, such as cancer (Antolin *et al.,* 2016).

Regarding the lung cancer EGFR target (4HJO), all ligands except for 5 exhibited binding affinities ranging from -6.5 to -8.9 kcal/mol. The 2-pyrazolin-5-ol, 1-acetyl-5-perfluorooctyl-3-methyl- (C25) demonstrated the strongest interaction at -8.9 kcal/mol, characterized by a pair of hydrogen bonds shared between Lys721 and Gly700, in comparison to erlotinib (Table 6). A similar pattern was observed for the cancer-specific nuclear and kinase receptors. The same pyrazoline derivative once again ranked highest for breast cancer ERα (3ERT) and prostate cancer AR (1E3G), with binding affinities of -8.6 and -8.8 kcal/mol, respectively (Table 7), surpassing conventional tamoxifen (-6.3 kcal/mol) and bicalutamide (-6.5 kcal/mol). Additionally, regarding (3PP0) HER2 stomach cancer target, the compound demonstrated a favorable docking score of -9.6 kcal/mol and formed seven hydrogen bonds with Asp863, Arg849, Ser728, Thr862, and Thr798, this

Table 5. Molecular docking analysis of selected compounds against PDB ID: 3KK6 (COX-1) and PDB ID: 3LN1 (COX-2), highlighting binding affinities, hydrogen bond interactions, and key interacting residues.

Sl. No.	Compounds	COX-1 PDB ID: 3KK6			COX-2 PDB ID: 3LN1		
		Binding Affinity (kcal/mol)	H-Bonds	Residues H-bonding	Binding affinity (kcal/mol)	H-Bonds	Residues H- bonding
1	Verimol K	-7.8	1	ILE 523	-8.1	1	SER 516
3	8-Deoxylactucin	-7.2	1	LEU 352	-7.9	1	TYR 341
4	(E)-3,3'-Dimethoxy-4,4'-dihydroxystilbene	-7.4	1	ARG 120	-7.2	2	ARG 499 HIS 75
5	1-(2,4-Dihydroxyphenyl)-2-(4-methoxy-3-nitrophenyl)ethanone	-7.3	3	TYR 385 SER 530 MET 522	-8.4	4	MET 508 ARG 106 TYR 371 SER 516
6	N-Benzyloxy-2,2-bis(trifluoromethyl)aziridine	-7.5	2	ARG 120	-8.6	1	SER 516
7	L-Alanine, N-benzoyl-, methyl ester	-7.1	1	SER 353	-8.4	2	ARG 106 TYR 341
8	Phthalic acid, di(6-methylhept-2-yl) ester	-	-	-	-8.5	2	HIS 75 ARG 499
9	Pentafluoropropionic anhydride	-	-	-	-7.7	2	TYR 341 ARG 106
10	3-Methylbenzoic acid, 2-formyl-4,6-dichlorophenyl ester	-	-	-	-8.5	1	SER 516
11	5-(2,2,2-Tri(2-cyanoethyl)acetyl)-2-methylpyridine	-	-	-	-8.3	2	TYR 341 ARG 106
12	Diethylmalonic acid, diphenethyl ester	-	-	-	-8.6	2	TYR 341 ARG 106
13	4,4'-Difluorobenzil	-	-	-	-9.2	1	HIS 75
14	3-Hydroxy-4-methoxycinnamic acid	-7	3	SER 353 TYR 355 MET 522	-7.7	4	ALA 513 MET 508 ARG 499 LEU 338
15	L-Phenylalanine, N-acetyl-, methyl ester	-	-	-	-7.1	2	ALA 513 TYR 341
16	9-Octadecenoic acid	-7	1	SER 530	-6.7	1	SER 339
17	Octadecanoic acid	-	-	-	-6.8	2	LEU 338 GLN 178
18	9,12,15-Octadecatrienoic acid, methyl ester, (Z,Z,Z)-	-	-	-	-7.2	2	TYR 341 ARG 106
19	p-Coumaric acid	-6.6	2	TYR 355 LEU 352	-7	2	ARG 499 SER 339
20	(9E,11E)-Octadecadienoic acid	-6.6	1	SER 530	-6.8	1	VAL 102
21	9-Octadecenoic acid, methyl ester, (E)-	-	-	-	-6.7	1	ARG 106
22	n-Hexadecanoic acid				-6.8	1	ARG 499
23	Methyl stearate	-6.7	1	SER 530			
24	9,12-Octadecadienoic acid (Z,Z)-, methyl ester	-	-	-	-7.1	2	ARG 106 TYR 341
25	Hexadecanoic acid, methyl ester	-6.5	1	SER 530	-	-	-
26	Z-(13,14-Epoxy)tetradec-11-en-1-ol acetate	-	-	-	-7.2	2	HIS 75 ARG 499
27	Citronellyl butyrate	-6.6	1	ARG 120	-	-	-
28	Curcumenol				-7.2	1	ALA 513
29	9,12,15-Octadecatrienoic acid, 2,3-dihydroxypropyl ester, (Z,Z,Z)-	-6.7	1	LEU 352 SER 353	-7.7	3	GLN 178 LEU 338 HIS 75
30	E-6-Octadecen-1-ol acetate	-	-	-	-7	1	HIS 75
31	Innuchenenolide C	-	-	-	-8	2	ARG 499 SER 516
32	2,4-Bis(dimethylbenzyl)-6-t-butylphenol	-	-	-	-7	1	GLN 336
33	2-Pyrazolin-5-ol, 1-acetyl-5-perfluoroctyl-3-methyl-	-	-	-	-10	2	TYR 341 MET 508
34	9-Octadecene, 1,1-dimethoxy-, (Z)-	-6.7	1	SER 530	-	-	-

Table 6. Molecular docking analysis of selected compounds with PDB ID: 4HJO (Lung Cancer) and PDB ID: 3KK6 (Mu Central), highlighting binding affinities, hydrogen bond interactions, and key interacting residues.

Sl. No.	Compounds	Lung cancer			Mu central		
		PDB ID: 4HJO			PDB ID: 4DKL		
		Binding Affinity (kcal/mol)	H-Bonds	Residues H-bonding	Binding affinity (kcal/mol)	H-Bonds	Residues H-bonding
1	Verimol K	-8.1	1	THR 766	-6 A green	1	SER 60
2	8-Deoxylactucin	-8.4	1	THR 766	-7.5	1	TRP 318
3	(E)-3,3'-Dimethoxy-4,4'-dihydroxystilbene	-	-	-	-6.7	1	HIS 54
4	1-(2,4-Dihydroxyphenyl)-2-(4-methoxy-3-nitrophenyl)ethanone	-8	3	ALA 719 THR 766 LYS 721	-6.2	1	HIS 54
5	N-Benzyloxy-2,2-bis(trifluoromethyl)aziridine	-8.2	2	PHE 832 ASP 831	-5.4	1	CYS 321
6	L-Alanine, N-benzoyl-, methyl ester	-6.5	1	ARG 817	-	-	-
7	Phthalic acid, di(6-methylhept-2-yl) ester	-7.3	1	THR 830	-	-	-
8	Pentafluoropropionic anhydride	-7.5	6	THR 766 ASP 831 PHE 832 THR 830	-	-	-
9	3-Methylbenzoic acid, 2-formyl-4,6-dichlorophenyl ester	-8.3	2	THR 830 LYS 721	-	-	-
10	5-(2,2,2-Tri(2-cyanoethyl)acetyl)-2-methylpyridine	-6.7	4	LYS 851 GLY 700 ARG 817 LYS 721	-	-	-
11	Diethylmalonic acid, diphenethyl ester	-7.3	2	LYS 721	-	-	-
12	4,4'-Difluorobenzil	-8.3	2	THR 830 THR 766	-6.8	1	TRP 318
13	3-Hydroxy-4-methoxycinnamic acid	-6.5	2	LYS 721	-5.7 C pink	3	ASN 127 GLN 124 TYR 75
14	9-Octadecenoic acid	-6.7	1	ASP 831	-5.7 D BLUE	3	LEU A219 GLU 229 SER 533
15	9,12,15-Octadecatrienoic acid, methyl ester, (Z,Z,Z)-	-6.7	3	CYS 751 ASP 831	-5.6	1	HIS 54
16	p-Coumaric acid				-5.5	1	ASN 127
17	(9E,11E)-Octadecadienoic acid	-6.8	2	CYS 751 PHE 832			
18	n-Hexadecanoic acid	-	-	-	-5.3	2	TYR 75 HIS 319
19	Methyl stearate	-	-	-	-5.3	1	ASN 127
20	9,12-Octadecadienoic acid (Z,Z)-, methyl ester	-6.5	1	ASP 831	-	-	-
21	Z-(13,14-Epoxy)tetradec-11-en-1-ol acetate	-6.5	2	MET 769 LEU 753	-5.4	3	ASN 127 TYR 75 HIS 54
22	Citronellyl butyrate	-6.6	1	THR 766	-5.3	1	ASN 127
23	Curcumenol	-	-	-	-6.1	1	TYR 299
24	9,12,15-Octadecatrienoic acid, 2,3-dihydroxypropyl ester, (Z,Z,Z)-	-6.8	3	CYS 751 ASP 831 PHE 832	-	-	-
25	E-6-Octadecen-1-ol acetate	-6.6	2	ASP 831 PHE 832	-	-	-
26	Innuchenenolide C	-7.6	2	LYS 721 MET 769	-	-	-
27	2,4-Bis(dimethylbenzyl)-6-t-butylphenol	-8.6	1	ASP 813	-6.3 B RED	1	ALA 22
28	2-Pyrazolin-5-ol, 1-acetyl-5-perfluoroctyl-3-methyl-	-8.9	2	LYS 721 GLY 700	-6.2 C yellow	1	TYR 151
29	.gamma.-Sitosterol	-8.9	1	PRO 890	-6.2 d blue	2	GLN 25 ALA 22
30	2-Naphthyl methyl ketone	-7.4	1	LYS 721	-6.6	1	TYR 299

Table 7. Molecular docking analysis of selected compounds against PDB ID: 3ERT (Breast Cancer) and PDB ID: 1E3G (Prostate Cancer), highlighting binding affinities, hydrogen bond interactions, and key interacting residues.

Sl. No.	Compounds	Breast cancer			Prostate cancer		
		PDB ID: 3ERT			PDB ID: 1E3G		
		Binding Affinity (kcal/mol)	H-Bonds	Residues H-bonding	Binding affinity (kcal/mol)	H-Bonds	Residues H- bonding
1	Verimol K	-7.2	1	LEU 346	-	-	-
2	8-Deoxylactucin	-	-	-	-7.1	1	THR 877
3	(E)-3,3'-Dimethoxy-4,4'-dihydroxystilbene	-6.8	-	-	-7.3	3	LYS 808 GLN 711 TRP 751
4	1-(2,4-Dihydroxyphenyl)-2-(4-methoxy-3-nitrophenyl)ethanone	-	-	-	-8	5	ASN 756 THR 755 ARG 752 GLN 711
5	N-Benzyloxy-2,2-bis(trifluoromethyl)aziridine	-7.9	1	ARG 394	-8.4	1	THR 877
6	L-Alanine, N-benzoyl-, methyl ester	-	-	-	-6.9	2	ARG 752 LYS 808
7	Pentafluoropropionic anhydride	-6.9	1	ARG 394	-	-	-
8	5-(2,2,2-Tri(2-cyanoethyl)acetyl)-2-methylpyridine	-6.8	2	THR 347 ARG 394	-6.5	3	ARG 752 THR 877 GLN 711
9	4,4'-Difluorobenzil	-8	1	ARG 394	-8.5	1	ARG 752
10	3-Hydroxy-4-methoxycinnamic acid	-6.2	1	ARG 394	-6.9	3	LEU 704 GLN 711 ARG 752 MET 745
11	9-Octadecenoic acid	-	-	-	-6.5	2	ARG 752 GLN 711
12	9,12,15-Octadecatrienoic acid, methyl ester, (Z,Z,Z)-	-	-	-	-6.5	1	LEU 701
13	p-Coumaric acid	-	-	-	-7	3	ASN 705 ARG 752 GLN 711
14	(9E,11E)-Octadecadienoic acid	-6.6	1	GLU 353	-	-	-
15	9-Octadecenoic acid, methyl ester, (E)-	-	-	-	-6.5	2	ARG 752 GLN 711
16	Citronellyl butyrate	-6.1	1	ARG 394	-	-	-
17	Curcumenol	-7.5	1	THR 347	-	-	-
18	9,12,15-Octadecatrienoic acid, 2,3-dihydroxypropyl ester, (Z,Z,Z)-	-6.4	2	ALA 350 GLU 353	-	-	-
19	E-6-Octadecen-1-ol acetate	-6.3	2	ARG 394	-	-	-
20	2-Pyrazolin-5-ol, 1-acetyl-5-perfluoroctyl-3-methyl-	-8.6	1	ASP 351	-8.8	6	ARG 752 LYS 808
21	2-Naphthyl methyl ketone	-7.1	2	ARG 394	-	-	-
22	N-Acetyl-phenylalanine methylester	-6.6	-	-	-6.6	3	VAL 685 GLY 683 ARG 752
23	Salicyl hydrazide	-6.4	2	ARG 394 GLU 353	-6.5	3	PRO 682 GLY 683 ARG 752
24	Lactose	-6.3	2	LEU 346 GLU 353	-6.8	3	GLY 683 ARG 752 LYS 808
25	Coniferyl aldehyde	-	-	-	-6.8	1	GLN 711
26	5-Formyl-2-methoxyphenyl acetate	-	-	-	-6.5	2	ARG 752 GLN 711

Table 8. Molecular docking analysis of selected compounds against PDB ID: 3PP0 (Stomach Cancer) and PDB ID: 5F19 (Colorectal Cancer), highlighting binding affinities, hydrogen bond interactions, and key interacting residues.

Sl. No.	Compounds	Stomach cancer			Colorectal cancer		
		PDB ID: 3PP0			PDB ID: 5F19		
		Binding Affinity (kcal/mol)	H-Bonds	Residues H-bonding	Binding affinity (kcal/mol)	H-bond	Residues H-Bonding
1	Verimol K	-8.8	2	SER 783 ASP 863	-8.1	2	PHE 529 LEU 531
2	8-Deoxylactucin	-8.9	2	CYS 805 THR 862	-8.9	1	LEU 531
3	(E)-3,3'-Dimethoxy-4,4'-dihydroxystilbene	-	-	-	-7.8	1	PHE 529
4	1-(2,4-Dihydroxyphenyl)-2-(4-methoxy-3-nitrophenyl)ethanone	-9.4	2	THR 798 SER 783	-8.9	2	ARG 120 TYR 355
5	N-Benzyloxy-2,2-bis(trifluoromethyl)aziridine	-8.7	1	THR 798 SER 783	-	-	-
6	Phthalic acid, di(6-methylhept-2-yl) ester	-8.7	1	THR 682	-	-	-
7	Pentafluoropropionic anhydride	-8.5	3	ASP 863 SER 728 THR 862	-7.7	3	LEU 531 PHE 529
8	3-Methylbenzoic acid, 2-formyl-4,6-dichlorophenyl ester	-8.9	1	THR 862	-	-	-
9	5-(2,2,2-Tri(2-cyanoethyl)acetyl)-2-methylpyridine	-7.3	2	MET 801 CYS 805	-7.8	3	TYR 355 ARG 120 TYR 385
10	Diethylmalonic acid, diphenethyl ester	-9	3	ASP 863 SER 783 THR 798	-	-	-
11	4,4'-Difluorobenzil	-9.2	2	SER 783 THR 798	-9.1	1	LEU 531
12	3-Hydroxy-4-methoxycinnamic acid	-7	2	ALA 751 LYS 753	-7.1	3	LEU 531 TYR 385
13	L-Phenylalanine, N-acetyl-, methyl ester	-7.4	2	SER 783 ASP 863	-	-	-
14	9-Octadecenoic acid	-7.3	1	MET 801	-7.2	1	TYR 355
15	9,12,15-Octadecatrienoic acid, methyl ester, (Z,Z,Z)-	-7.4	3	SER 783 ASP 863	-7.7	1	TYR 355
16	(9E,11E)-Octadecadienoic acid	-7.7	1	MET 801	-7.4	2	TYR 355
17	n-Hexadecanoic acid	-7	2	MET 801	-	-	-
18	9,12-Octadecadienoic acid (Z,Z)-, methyl ester	-7.6	1	CYS 805	-7.1	3	GLY 533 LEU 534 LEU 531
19	Citronellyl butyrate	-	-	-	-7.1	4	LEU 531 LEU 534 GLY 533
20	Curcumenol	-	-	-	-8.5	1	TYR 385
21	9,12,15-Octadecatrienoic acid, 2,3-dihydroxypropyl ester, (Z,Z,Z)-	-7.5	3	ASP 863 SER 783	-7.7	1	TYR 355
22	E-6-Octadecen-1-ol acetate	-7	2	THR 798 SER 783	-	-	-
23	Innuchenenolide C	-7.5	2	THR 632 SER 728	-8.4	2	PHE 529 TYR 355
24	2-Pyrazolin-5-ol, 1-acetyl-5-perfluoroctyl-3-methyl-	-9.6	7	ASP 863 ARG 849 SER 728 THR 862 THR 798	-11.9	5	LEU 531 PHE 529 LEU 352
25	2-Naphthyl methyl ketone	-8.2	2	ASP 863 SER 862	-7.8	2	LEU 531 PHE 529
26	Lactose	-7.8	4	ASP 863 ALA 751 LEU 796	-	-	-
27	D-Alanine, N-propargyloxycarbonyl-, propargyl ester	-7.4	4	THR 798 THR 862 ASP 863 SER 783	-	-	-
28	Benzoic acid, 3,4,5-trihydroxy-, methyl ester	-7.3	1	THR 862	-	-	-
29	N-Acetyl-phenylalanine methylester	-7.2	1	THR 862	-	-	-
30	Sarcosine, n-propargyloxycarbonyl-, propargyl ester	-7	3	THR 862 ASP 863 SER 783	-	-	-

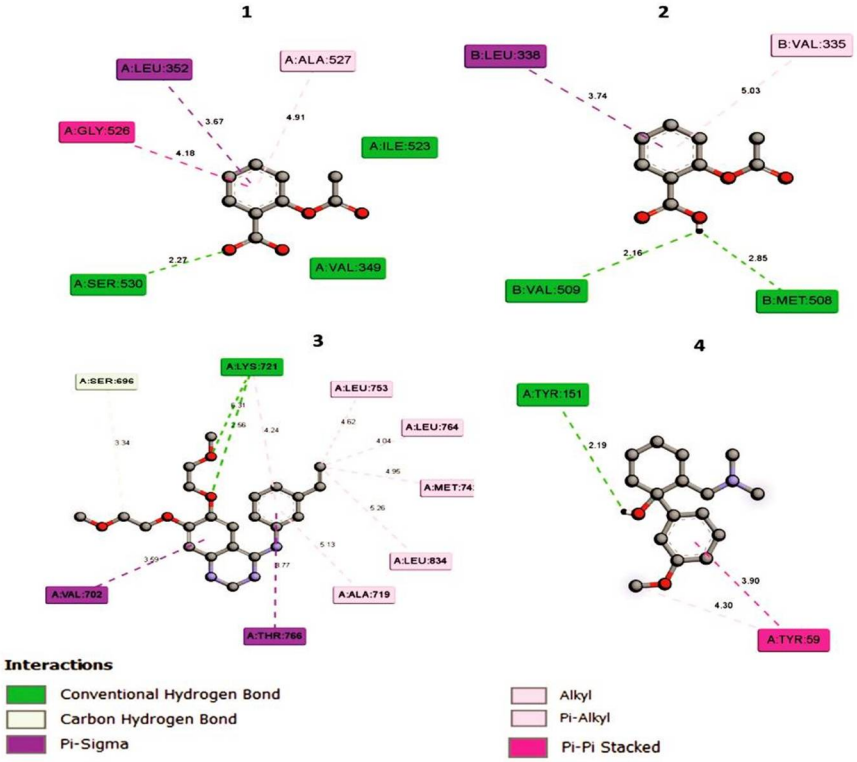

Figure 3. Docking interactions of standard drugs with selected protein receptors: (1) Aspirin–COX-1 (3KK6), (2) Aspirin–COX-2 (3LN1), (3) Erlotinib-Lung Cancer (4) Tramadol–μ-Opioid Receptor (4DKL).

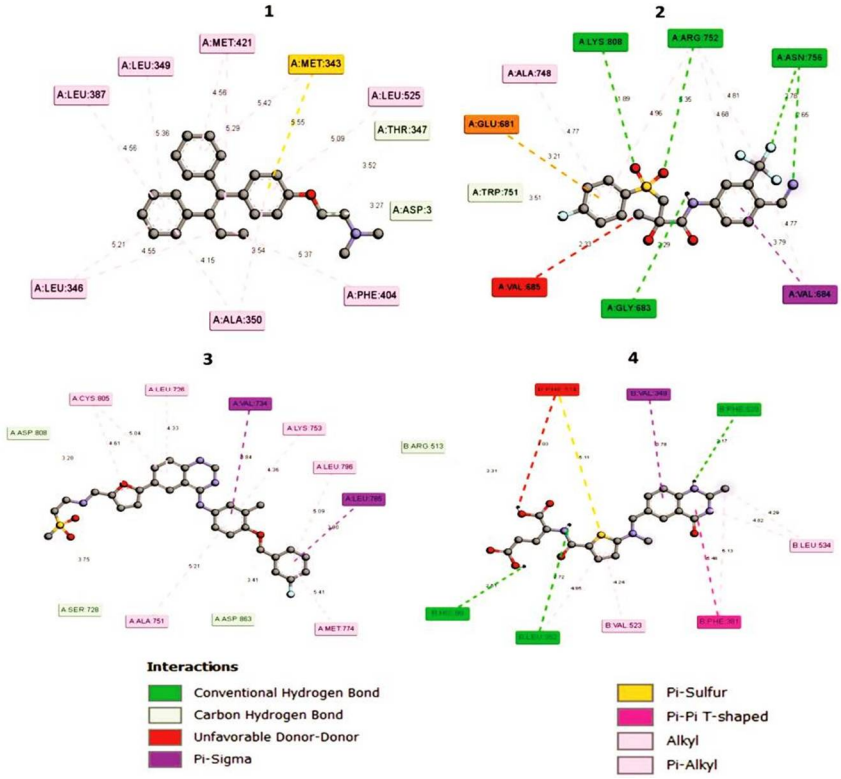

Figure 4. Docking interactions of standard drugs with selected protein receptors: (1) Tamoxifen- breast cancer ER, (2) Bicalutamide-prostate cancer AR, (3) Lapatinib-stomach cancer target (PDB: 3PP0) and (4) Raltitrexed-colorectal cancer CDK8 (PDB: 5F19).

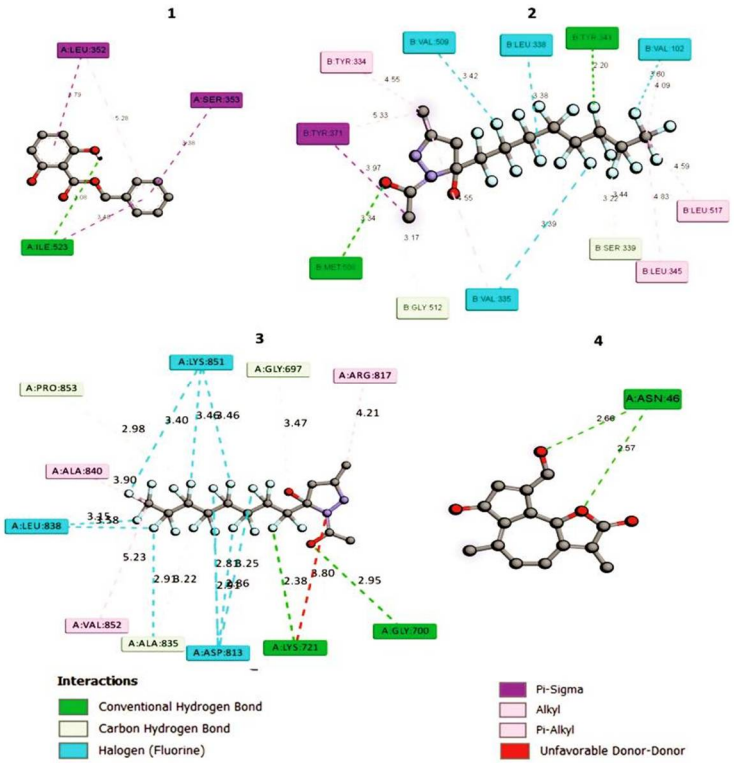

Figure 5. Molecular docking interactions of selected ligands with multiple therapeutic targets: (1) COX-1 (PDB: 3KK6) with Verimol K, (2) COX-2 (PDB: 3LN1) with C25, (3) Lung cancer target EGFR (PDB: 4HJO) with C25, (4) μ-Opioid receptor3 (PDB: 4DKL) with 8-Deoxylactucin.

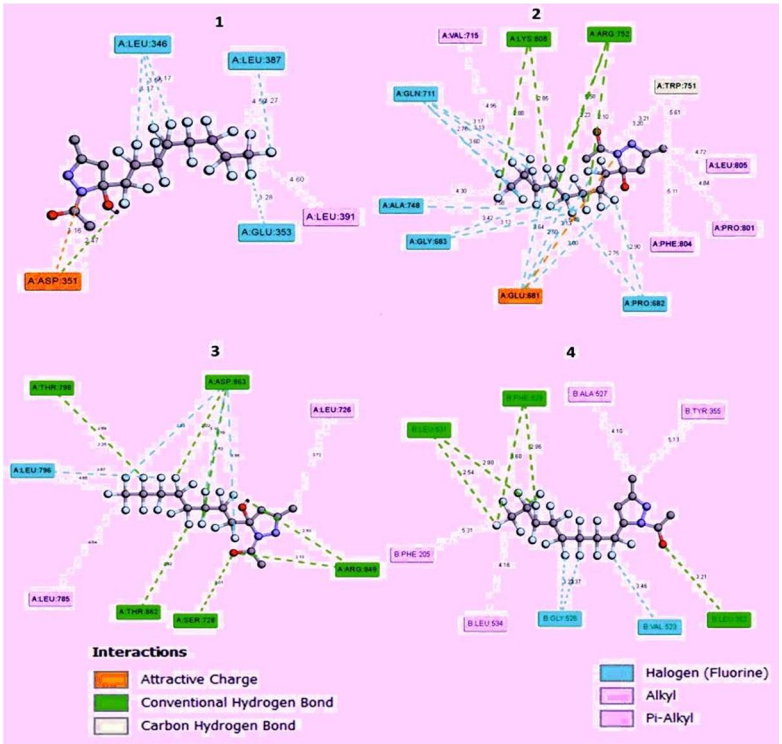

Figure 6. Molecular docking interactions of selected ligands with multiple therapeutic targets: (1) Breast cancer ERα (PDB: 3ERT) with C25 (2) Prostate cancer AR (PDB: 1E3G) with C25, (3) Stomach Cancer target (PDB: 3PP0) with C25 and (4) Colorectal cancer CDK8 (PDB: 5F19) with C25.

performance surpasses that of standard lapatinib (-9.9 kcal/mol). The most favorable activities were observed for the colorectal cancer CDK8 (5F19), where the C25 ligand demonstrated a binding affinity of -11.9 kcal/mol, engaging five HBA interactions (notable contacts: Leu531, Phe529 and Leu352). This performance surpasses that of the standard drug raltitrexed listed in Table 8 and Figure (3, 4, 5, 6) which exhibits a binding affinity of -9.5 kcal/mol. Together, the data presented highlight the multi-target binding potential of (C25) and its superior performance compared to clinically relevant standard drugs across numerous anti-inflammatory, analgesic, and anticancer targets. This aligns with recent research indicating that these fluorinated pyrazoline derivatives demonstrate enhanced lipophilicity, membrane permeability and binding-site complementarity, making them appropriate scaffolds for the design of multi-target drugs (Nadigar *et al.*, 2024, Wang *et al.*, 2023). Although docking results do not guarantee biological activity, similar binding patterns across eight targets suggest that this lead possesses promising potential as a drug candidate. Further investigations will employ molecular dynamics simulations, MM/PBSA binding free energy calculations, and *in vitro* enzymatic assays to validate the interactions, as well as assess cell-based antiproliferative and anti-inflammatory activities. Overall, the current report provides an excellent computational foundation for designing pyrazoline analogs as prospective multi-target therapeutics.

Conclusion

We identified that 2-pyrazolin-5-ol, 1-acetyl-5-perfluorooctyl-3-methyl (C25), is a potential multi-target inhibitor showing favorable predicted binding affinities toward inflammatory proteins and oncogenes. Steady-state docking calculations revealed that the compound exhibited a higher binding affinity than conventional reference drugs such as aspirin, erlotinib, tamoxifen, bicalutamide, lapatinib and raltitrexed. It also formed multiple hydrogen bonding interactions within major catalytic and regulatory pockets. Furthermore, it demonstrates potent inhibitory activity against COX-1/COX-2, EGFR, ERα, AR, and CDK8, as well as clinical relevance for stomach cancer. This suggests that the scaffold has potential for further development as a dual anti-inflammatory and anticancer property. Although mu opioid receptor binding was moderate, its affinity exceeded that of tramadol, a conventional analgesic, indicating potential for additional neuromodulatory effects. Overall, these findings underscore the potential of fluorinated pyrazoline derivatives as predicted multi-target scaffolds capable of interacting with diverse disease-related proteins. Although the *in silico* results appear promising, these findings must be comprehensively validated through targeted *in vitro* assays, *in vivo* preclinical studies, and eventual clinical trials to establish therapeutic efficacy and safety. Overall, these findings establish a preliminary computational basis for the future optimization and preclinical evaluation of this scaffold as a potential, multi-targeted therapeutic candidate.

Author Contribution

Conceptualization: Farhad Hossain; Supervision: Farhad Hossain; Methodology: Farhad Hossain, Mst. Neha Islam Ema; Investigation: Mst. Neha Islam Ema, A B M Ashraful, Kanij Fatema, Saikat Bhowmik; Data curation: Mst. Neha Islam Ema, A B M Ashraful, Kanij Fatema, Saikat Bhowmik; Formal analysis: Mst. Neha Islam Ema, Farhad Hossain; Writing original draft: Mst. Neha Islam; Ema, A B M Ashraful; Writing - Review and Editing: AHM Khurshid Alam, Farhad Hossain.

Funding

No funds have been received to conduct this study.

Conflicts of Interest

There are no conflicts of interest that the authors have disclosed concerning the publication of this paper.

Acknowledgement

The authors are grateful to the Department of Pharmacy, State University of Bangladesh, Bangladesh, for providing the resources needed to conduct this project.

References

Agu, P. C., Afiukwa, C. A., Orji, O., Ezeh, E., Ofoke, I., Ogbu, C., Ugwuja, E. I. and Aja, P. 2023. Molecular docking as a tool for the discovery of molecular targets of nutraceuticals in diseases management. *Sci. Rep.* **13**, 13398.

Ahmadi, M., Bekeschus, S., Weltmann, K.-D., von Woedtke, T. and Wende, K. 2022. Non-steroidal anti-inflammatory drugs: recent advances in the use of synthetic COX-2 inhibitors. *RSC Med. Chem.* **13**, 471-496.

Anighoro, A., Bajorath, J. and Rastelli, G. 2014. Polypharmacology: challenges and opportunities in drug discovery: miniperspective. *J. Med. Chem.* **57**, 7874-7887.

Antolin, A. A., Workman, P., Mestres, J. and Al-Lazikani, B. 2016. Polypharmacology in precision oncology: current applications and future prospects. *Curr. Pharm. Des.* **22**, 6935-6945.

Azad, I. 2023. Molecular docking in the study of ligand–protein recognition: an overview. In: *Molecular Docking – Recent Advances* (Azad, I., Ed.), Springer, Cham, pp. 1-25.

Baroroh, U., Biotek, M., Muscifa, Z. S., Destiarani, W., Rohmatullah, F. G. and Yusuf, M. 2023. Molecular interaction analysis and visualization of protein–ligand docking using Biovia Discovery Studio Visualizer. *Indones. J. Comput. Biol.* **2**, 22-30.

Berman, H. M., Westbrook, J., Feng, Z., Gilliland, G., Bhat, T. N., Weissig, H., Shindyalov, I. N. and Bourne, P. E. 2000. The protein data bank. *Nucleic Acids Res.* **28**, 235-242.

Dallakyan, S. and Olson, A. J. 2014. Small-molecule library screening by docking with PyRx. In: *Chemical Biology: Methods and Protocols* (Hempel, J., Williams, C. H. and Hong, C. C., Eds.), Springer, New York, pp. 243-250.

Edache, E. I., Uzairu, A., Mamza, P. A., Shallangwa, G. A., Yagin, F. H., Abdel Samee, N. and Mahmoud, N. F. 2023. Combining docking, molecular dynamics simulations, ADMET pharmacokinetics properties, and MMGBSA calculations to create specialized protocols for virtual screening campaigns on autoimmune disorder and SARS-CoV-2 main protease. *Front. Mol. Biosci.* **10**, 1254230.

Ghaffar, S. A., McCarter, M. D., Kim, S. S., Bilal, M., Del Chiaro, M. and Mungo, B. 2025. Advances in the management of gastric cancer. *BMJ* **391**, e079123.

Goodsell, D. S., Sanner, M. F., Olson, A. J. and Forli, S. 2021. The AutoDock suite at 30. *Protein Sci.* **30**, 31-43.

Greten, F. R. and Grivennikov, S. I. 2019. Inflammation and cancer: triggers, mechanisms, and consequences. *Immunity* **51**, 27-41.

Guex, N., Peitsch, M. C. and Schwede, T. 2009. Automated comparative protein structure modeling with SWISS-MODEL and Swiss-PdbViewer: a historical perspective. *Electrophoresis* **30**, S162-S173.

Jordan, V. C. 2021. Turning scientific serendipity into discoveries in breast cancer research and treatment: a tale of PhD students and a 50-year tamoxifen team. *Breast Cancer Res. Treat.* **190**, 1938.

Ju, Z., Li, M., Xu, J., Howell, D. C., Li, Z. and Chen, F. E. 2022. Recent development on COX-2 inhibitors as promising anti-inflammatory agents: the past 10 years. *Acta Pharm. Sin. B* **12**, 2790-2807.

Kim, S., Chen, J., Cheng, T., Gindulyte, A., He, J., He, S., Li, Q., Shoemaker, B. A., Thiessen, P. A. and Yu, B. 2019. PubChem 2019 update: improved access to chemical data. *Nucleic Acids Res.* **47**, D1102-D1108.

Kim, S., Thiessen, P. A., Bolton, E. E., Chen, J., Fu, G., Gindulyte, A., Han, L., He, J., He, S. and Shoemaker, B. A. 2016. PubChem substance and compound databases. *Nucleic Acids Res.* **44**, D1202-D1213.

Kitchen, D. B., Decornez, H., Furr, J. R. and Bajorath, J. 2004. Docking and scoring in virtual screening for drug discovery: methods and applications. *Nat. Rev. Drug Discov.* **3**, 935-949.

Kourat, O., Benhalima, N., Al-Dies, A.-A. M., Guendouzi, A., Benyahlou, Z. D., Megrouss, Y., Drissi, M., Alem, G. A., Sindi, E. R. and Zaki, M. E. 2025. Structural, nonlinear optical, and molecular docking studies of Schiff base compounds as multi-target inhibitors of AChE, BChE, and carbonic anhydrases. *Sci. Rep.* **15**, 34818.

Lee, H.-M., Lee, H.-J. and Chang, J.-E. 2022. Inflammatory cytokine: an attractive target for cancer treatment. *Biomedicines* **10**, 2116.

Lin, T. E., Yang, C. R., Chou, C. H., Hsu, J. Y., Chao, M. W., Sung, T. Y., Hsieh, J. H., Huang, W. J. and Hsu, K. C. 2022. Discovery of a novel cyclin-dependent kinase 8 inhibitor with an oxindole core for anti-inflammatory treatment. *Biomed. Pharmacother.* **146**, 112459.

Millanta, F., Asproni, P., Canale, A., Citi, S. and Poli, A. 2016. COX-2, mPGES-1 and EP2 receptor expression in mammary tumours. *Vet. Comp. Oncol.* **14**, 270–280.

Miotto, K., Cho, A. K., Khalil, M. A., Blanco, K., Sasaki, J. D. and Rawson, R. 2017. Trends in tramadol: pharmacology, metabolism, and misuse. *Anesth. Analg.* **124**, 44-51.

Morris, G. M., Huey, R., Lindstrom, W., Sanner, M. F., Belew, R. K., Goodsell, D. S. and Olson, A. J. 2009. AutoDock4 and AutoDockTools4: automated docking with selective receptor flexibility. *J. Comput. Chem.* **30**, 2785-2791.

Nadigar, S., Gattu, R., Ramesh, S., Dharmappa, R. N., Nanjundaswamy, V. K. and Ramesh, S. 2024. A novel class of potent antiangiogenic and antioxidant pyrazoles: synthesis, bioactivity, docking and ADMET studies. *Future Med. Chem.* **16**, 2285-2300.

Olsson, M. H., Søndergaard, C. R., Rostkowski, M. and Jensen, J. H. 2011. PROPKA3: consistent treatment of internal and surface residues in empirical pKa predictions. *J. Chem. Theory Comput.* **7**, 525-537.

Prado-Romero, D. L., Gómez-García, A., Cedillo-González, R., Villegas-Quintero, H., Avellaneda-Tamayo, J. F., López-López, E., Saldívar-González, F. I., Chávez-Hernández, A. L. and Medina-Franco, J. L. 2023. Consensus docking aid to model the activity of an inhibitor of DNA methyltransferase 1 inspired by de novo design. *Front. Drug Discov.* **3**, 1261094.

Remon, J. and Hendriks, L. E. 2021. Targeted therapies for unresectable stage III non-small cell lung cancer. *Mediastinum* **5**, 22.

Ricciotti, E. and Fitzgerald, G. A. 2011. Prostaglandins and inflammation. *Arterioscler. Thromb. Vasc. Biol.* **31**, 986-1000.

Sokołowska, P., Bleibel, L., Owczarek, J. and Wiktorowska-Owczarek, A. 2024. PPARγ, NF-κB and UPR pathway as molecular targets in NSAIDs action. *Adv. Clin. Exp. Med.* **33**, 1007-1022.

Trott, O. & Olson, A. J. 2010. Auto Dock Vina: improving speed and accuracy of docking. *J. Comput. Chem.* **31**, 455-461.

Uddin, A., Gupta, S., Mohammad, T., Shahi, D., Hussain, A., Alajmi, M. F., El-Seedi, H. R., Hassan, I., Singh, S. and Abid, M. 2022. Target-based virtual screening identifies a potent antimalarial. *Front. Pharmacol*. **13**, 850176.

Wang, Z., Felstead, H. R., Troup, R. I., Linclau, B. and Williamson, P. T. F. 2023. Lipophilicity modulations by fluorination correlate with membrane partitioning. *Angew. Chem. Int. Ed.* **62**, e202301077.

Wangzhou, A., Paige, C., Neerukonda, S. V., Naik, D. K., Kume, M., David, E. T., Dussor, G., Ray, P. R. and Price, T. J. 2021. Ligand–receptor interactome platform for discovery of pain mechanisms. *Sci. Signal.* **14**, eabe1648.

Wen, Y., Zhu, Y., Zhang, C., Yang, X., Gao, Y., Li, M., Yang, H., Liu, T. and Tang, H. 2022. Chronic inflammation, cancer development and immunotherapy. *Front. Pharmacol.* **13**, 1040163.

Yin, X., He, Z., Chen, K., Ouyang, K., Yang, C., Li, J., Tang, H. and Cai, M. 2024. Impact of CDK8 on tumor progression. *Front. Pharmacol*. **15**, 1386929.

Yuan, D., Wang, Z., Li, B., Li, X., Wang, Y., Wang, X., Cao, J., Guo, Y., Du, H. and Lu, S. 2023. Complexation of apigenin and oxymatrine enhances anti-inflammatory activity. *J. Nat. Prod.* **86**, 1179-1188.

Zhao, H. 2024. Structure-based virtual screening. *ACS Med. Chem. Lett.* **15**, 436-440.